Connectivity at the hillslope scale: Identifying interactions between storm size, bedrock permeability, slope angle and soil depth

L. Hopp *, J.J. McDonnell

Department of Forest Engineering, Resources and Management, Oregon State University, Corvallis, OR, USA

ARTICLE INFO

SUMMARY

The links between soil water movement at the plot scale and runoff generation at the hillslope scale are highly non-linear and still not well understood. As such, a framework for the general characterization of hillslopes is still lacking. Here we present a number of virtual experiments with a 3D physically-based finite element model to systematically investigate the interactions between some of the dominant controls on subsurface stormflow generation. We used the well-studied Panola experimental hillslope to test our base case simulation and used the surface and subsurface topography and the stormflow data of this site as a framework for a subsequent series of virtual experiments. The parameterization of the soil and bedrock properties was based on field measurements of soil moisture and saturated hydraulic conductivity. After calibration and testing against multiple evaluation criteria including distributed trench flow data and internal tensiometric response, we varied slope angle, soil depth, storm size and bedrock permeability across multiple ranges to establish a set of response surfaces for several hillslope flow metrics. We found that connectivity of subsurface saturation was a unifying descriptor of hillslope behavior across the many combinations of slope type. While much of the interplay between our four hillslope variables was intuitive, several interactions in variable combinations were found. Our analysis indicated that, e.g. interactions between slope angle, soil depth and storm size that caused unexpected behavior of hydrograph peak times were the result of the interplay between subsurface topography and the overlying soil mantle with its spatially varying soil depth distribution. Those interactions led to new understanding of process controls on connectivity .

Introduction

Field studies in hillslope hydrology in upland humid areas continue to characterize and catalogue the enormous heterogeneity and complexity of rainfall–runoff processes at different sites around the world. Nevertheless, the ability to generalize these findings to ungauged regions still remains largely out of reach (McDonnell et al., 2007). Hillslopes exhibit a baffling array of heterogeneity in landscape properties and complexity of their responses to fixed hillslope attributes (e.g. slope, soil depth, etc.) and temporally varying precipitation inputs. One common emergent feature at the hillslope scale appears to be the threshold response to storm rainfall and snowmelt inputs. These thresholds have been noted for decades (for early review see Dunne, 1978) and reported more recently at various hillslope trench investigations in Japan (e.g. Tani, 1997), New Zealand (e.g. Woods and Rowe, 1996), North America (e.g. Hutchinson and Moore, 2000) and Eur-

ope (e.g. Scherrer and Naef, 2003). Only recently have the process controls on threshold response been examined. Tromp-van Meerveld and McDonnell (2006a,b) demonstrated that connectivity of patches of transient saturation were a necessary prerequisite for exceeding the rainfall threshold necessary to drive lateral flow at the Panola Mountain research watershed in Georgia, USA. Since then, such connectivity has been modeled with percolation theory (Lehmann et al., 2007) and subsurface saturated connectivity has been shown to control hillslope response at other sites (Spence, 2007; van Verseveld et al., 2008).

Connectivity appears to be a possible unifying concept and theoretical platform for moving hillslope and watershed hydrology forward. Bracken and Croke (2007) have made compelling arguments for how connectivity may contribute, conceptually, to understanding surface runoff-dominated geomorphic systems. Their work follows similar calls in ecology for connectivity-based understanding of water-mediated transfers of matter, energy and organisms (Pringle, 2001). While biologists often define connectivity as the degree to which a landscape facilitates or impedes the movement of individuals (Taylor et al., 1993), a hillslope hydrological definition may be linked to how the hillslope architecture controls the filling and spilling of isolated patches of saturation,

* Corresponding author. Address: Department of Forest Engineering, Resources and Management, Oregon State University, 204 Peavy Hall, Corvallis, OR 97331-5706. Tel.: +1 541 737 8719; fax: +1 541 737 4316.

E-mail address: Luisa.Hopp@oregonstate.edu (L. Hopp).

leading to whole-slope connectedness of areas with high relative saturation. While this filling and spilling appears to be the mechanistic basis for threshold response in many landscapes (Gomi et al., 2008; Spence and Woo, 2006; Tromp-van Meerveld and McDonnell, 2006b; Buttle et al., 2004), these findings have been largely based on single case studies of individual hillslopes with little synthesis among and across sites. Such synthesis is made extremely difficult because the measurements made at different locations are often unique to that site.

Buttle (2006) pointed out the need to consider interactions between controls on hydrologic response instead of looking at controls and their effects individually. One possible way forward for synthetic work aimed at understanding the controls on hillslope connectivity and interactions among the many control factors are virtual experiments. Weiler and McDonnell (2004) defined virtual experiments as "numerical experiments driven by a collective field intelligence". We argue here that such an approach may help us begin to understand how different hillslope variables control the disposition of storm rainfall at the hillslope scale and influence ultimately whole-slope connectivity. While the list of possible variables is very long, some of the more important variables from recent field-based study of hillslope connectivity is soil depth (Buttle and McDonald, 2002), bedrock permeability (Onda et al., 2001) and topography (both surface and subsurface) (Freer et al., 2002). How different values and combinations of these static attributes combine with temporally varying storm rainfall characteristics is a major open research question in hydrology today. Virtual experiments offer a way to address such a question, where single-realization field study sites are unable to achieve this. More importantly, the virtual experiment approach may help identify and understand the interactions among these variables – something that hydrologists have not yet explored, yet clearly seen in nature.

Here we present a series of virtual experiments aimed at identifying the hillslope controls on connectivity. We use a physics-based model (Cloke et al., 2006; Ebel et al., 2008) to systematically explore the interactions between controlling hillslope variables and to surface the possible combinations of factors that might promote subsurface hydrological connectivity. We base our virtual experiments on a real hillslope that exhibits complex system behavior – the Panola experimental hillslope described previously by Freer et al. (2002) and many others – by first demonstrating that the model reproduces the hillslope response to a storm event from integrated flow measures at the slope base to internal, spatially distributed, process behavior within the hillslope. We then use that parameterization of the model for addressing questions aimed at understanding the interactions among what we consider to be some of the key variables controlling hillslope connectivity response to storm rainfall:

– How do factors inhibiting the generation of subsurface stormflow (e.g. the permeability of the underlying bedrock) interact with factors forcing the generation of subsurface stormflow (e.g. slope angle)?
– Is subsurface stormflow generation always positively correlated with slope angle and storm size, negatively correlated with bedrock permeability and soil depth or are there interactions between these factors?
– How does the connectivity of a transient water table at the soil–bedrock interface relate to interactions between factors?

We systematically varied each of our chosen variables to obtain 72 combinations for interaction analysis. Clearly, this list of variables is not complete and many other possible hillslope variables could be explored (e.g. spatial patterns of the rainfall input, rainfall intensity; slope length, topographic variability of the subsurface;

macroporosity, antecedent wetness, different soil types and hydraulic properties, soil layering, etc.). We chose our four factors as a starting point based on two constraints: findings from our previous field experiences at the Panola site (and elsewhere as noted above) and the realistic limitations of the model and associated computational time. This second aspect is somewhat analogous to decisions made in the field, where the extent of monitoring (in time and space) is decided based upon financial and manpower limitations.

Materials and methods

Study site and selected rainstorm event

The study hillslope that we used to define the geometry and the soil hydraulic properties of the model domain is part of the Panola Mountain Research Watershed (PMRW), situated in the Georgia Piedmont, 25 km southeast of Atlanta. The climate is subtropical-humid, with a mean annual air temperature of 16.3 °C and a mean annual rainfall of 1240 mm, distributed uniformly over the year. The study hillslope and the subsurface stormflow collection system have been described in detail elsewhere (Freer et al., 2002; Tromp-van Meerveld and McDonnell, 2006a,b). Here we only briefly describe the hillslope characteristics that are crucial for setting up the base case scenario of our virtual model environment.

The study hillslope has a slope angle of 13°. The upslope boundary consists of a small bedrock outcrop; the lower hillslope boundary is formed by a 20 m wide trench where subsurface stormflow from ten 2 m wide slope sections is continuously measured. Five soil pipes that have most likely developed from root decay are plumbed individually. The trench extends vertically to the interface between soil and bedrock. Lateral subsurface stormflow collected at the trench exfiltrates from the trench face through soil immediately overlying the bedrock (based on field observations by C. Graham, pers. com.). Surveyed surface and bedrock topography used in the model domain covers an area of 28 m by 48 m. The surface topography is relatively planar whereas the bedrock topography is highly irregular (Fig. 1b), resulting in variable soil depths ranging between 0 and 1.86 m, with a mean soil depth of 0.63 m and a coefficient of variation of 56%. The soil is a sandy loam, devoid of discernible structure or layering and overlain by a 0.15 m deep organic-rich horizon. The bedrock directly underlying the soil consists of 2–3 m of porous saprolite (soft disintegrated granite derived from the Panola granite beneath).

The model base case scenario that we used as a starting point for the virtual experiments was calibrated to the hydrologic response of the hillslope to a rainstorm that occurred on 6–7 March 1996. This is one of our best-studied storms in the Panola dataset (Burns et al., 2001; Freer et al., 2002; McDonnell et al., 1996). This 3-year return interval storm had a total precipitation amount of 87 mm over 31 h in two separate pulses (Fig. 1a). For this rainstorm, continuous pressure head readings exist from a tensiometer network distributed across the length of the trench and up to 30 m upslope of the trench (Freer et al., 2002). Fig. 1 shows the location and depth of tensiometers that were used for testing the model.

Virtual experiments

Base case scenario

We used the well known finite element model Hydrus-3D (Simunek et al., 2006) for our virtual experiments. This model numerically solves the Richards' equation for water flow in variably saturated porous media and has been used extensively in 1D and 2D forms for a variety of hydrological application (e.g. Buczko and Gerke, 2006; Kampf and Burges, 2007; Keim et al., 2006;
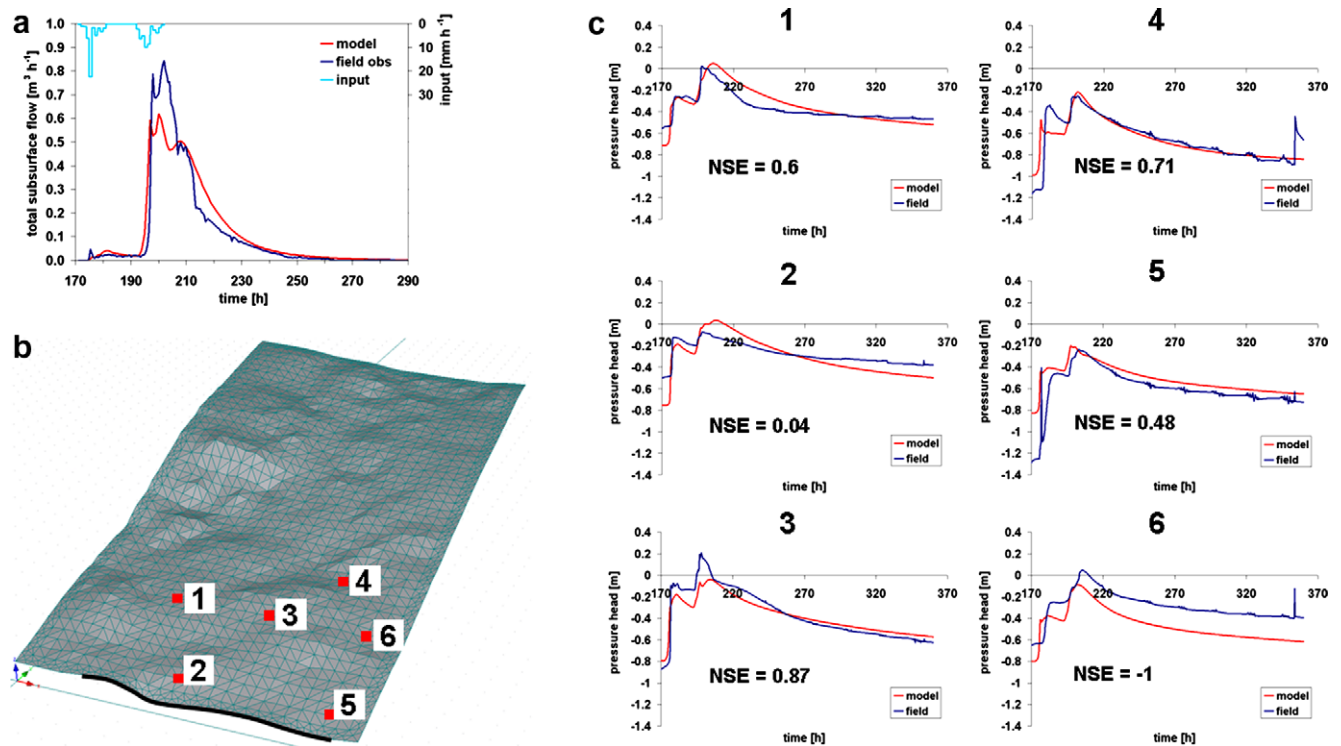
Fig. 1. Calibration and testing of the base case scenario. (a) Comparison between field and simulated hydrograph. The event starts at 171 h and ends at 202 h (total duration: 31 h). (b) Location of tensiometers and bedrock topography. All tensiometers were installed at the soil–bedrock interface (depth 0.5–0.6 m below the soil surface). Black bar denotes location of the 20 m wide trench. (c) Test of the model: comparison between field-measured and simulated pressure heads time series.

Sansoulet et al., 2008). The first step was to develop and calibrate a model setup that reproduced the general characteristics of the hydrologic response of the Panola study hillslope for the March 1996 rainstorm. We calibrated only to trench flow data. The objective of calibration was to obtain a model that behaved in a realistic way – consistent with our various forms of complementary field data – and not to build a model that exactly represents all of the complex flow processes that have been documented at Panola. In our search for a parameter set for the virtual experiments, our focus was exclusively on the 6–7 March 1996 response and we did not search for a unique parameter set that could be used for long-term hydrologic response modeling.

The model domain was generated by importing the Panola hillslope DEM (digital elevation model; x, y, z-coordinates of the surface and bedrock topography in 1 m resolution, interpolated from the surveyed 2 m grid), thus leading to the definition of two sublayers, one representing the soil and the other one the bedrock. The finite element mesh for the base case scenario contained 17,150 nodes, arranged in ten mesh layers and resulting in 29,484 3D elements in the form of triangular prisms (see Fig. S1 in the Supplementary information). The soil sublayer consisted of the topmost five mesh layers whereas the remaining lower five mesh layers belonged to the bedrock sublayer. Since the number of mesh layers was kept constant in each sublayer, the vertical spacing between mesh layers varied from a few mm where the soil is extremely shallow to approximately 90 cm in some regions of the bedrock. The average spacing between nodes in horizontal direction within one mesh layer was 1 m. The thickness of the entire model domain ranged from 1.74 to 4.11 m, depending on the topography. The transition into the deeper bedrock was represented by an inclined planar base surface. The bedrock sublayer in the model domain was assumed to represent the saprolite layer described in detail in Tromp-van Meerveld et al. (2007).

We chose a homogeneous description of the porous medium to keep the approach as parsimonious as possible. Although we know that soil pipe flow plays an important role for subsurface stormflow at this site (Tromp-van Meerveld and McDonnell, 2006a; Uchida et al., 2005), no substantial information regarding abundance, geometry and distribution of the soil pipes was available on which to base a parameterization of a dual-continuum approach. We therefore calibrated the model only to the flow that was measured at the ten 2 m trench sections, excluding pipe flow. We acknowledge that our representation of the hillslope is a gross simplification of a system that has evolved over long time spans as a result of interacting climatic, geomorphological and biological forces. Nevertheless, we are of the opinion that valuable insight into hillslope-scale subsurface stormflow generation can be gained with this simplified description of the hillslope.

Hydraulic properties of soil and bedrock were described with the van Genuchten–Mualem soil hydraulic model (van Genuchten, 1980). The van Genuchten parameters α and n were the only hydraulic parameters that were adjusted during the calibration process (Table 1). We specified the parameters θ_r (residual water content) and θ_s (saturated water content) based on long-term field observations of soil moisture ranges during dry and wet conditions (see Fig. 4 in Tromp-van Meerveld and McDonnell, 2006a), thus

Table 1
Soil hydraulic parameters used for the five materials of the model domain. Layers 1–5 represent the soil mantle, layers 6–10 the bedrock.

Material	Layers	θ_r (m^3 m^{-3})	θ_s (m^3 m^{-3})	α (m^{-1})	n (–)	K_s (m h^{-1})
1	1–2	0.28	0.475	4	2	3.5
2	3–4	0.28	0.46	4	2	1.5
3	5	0.325	0.45	4	2	0.65
4	6	0.3	0.45	3.25	1.75	0.006
5	7–10	0.28	0.4	3	1.5	0.0006

interpreting the difference between θ_r and θ_s as drainable porosity under prevailing moisture conditions. The soil was divided into three layers to account for the observed decrease of saturated hydraulic conductivity K_s in the profile as measured with field-based well permeametry on-site (Jim Freer, University of Bristol, pers. comm.). By doing this, we introduced anisotropy into the soil mantle, with hydraulic properties changing in vertical direction, i.e. with depth. The lowermost soil layer was represented by the saturated hydraulic conductivity K_s measured in a large, 30 cm diameter, undisturbed core taken near the study hillslope (McIntosh et al., 1999). The K_s values of the upper soil layers were specified such that the soil K_s decreased by a factor of five from the surface to the soil–bedrock interface. The bedrock was divided into two layers, with the upper one representing the highly weathered part of the bedrock layer and the lower one representing a transition into less weathered bedrock. In contrast to the often-made assumption of an impermeable bedrock underlying the soil on steeper hillslopes, we used the area-average effective conductivity of the weathered bedrock of approximately 6 mm h^{-1} (corresponding to 1.6×10^{-6} m s^{-1}) as estimated by Tromp-van Meerveld et al. (2007) as K_s value of the first bedrock layer. Thus, there was a contrast in saturated hydraulic conductivity between soil and bedrock of two orders of magnitude (Table 1). For the second bedrock layer we assumed K_s to be one order of magnitude lower.

An atmospheric boundary condition with hourly records of precipitation rates was imposed on the surface of the model domain. Evapotranspiration (ET) was considered to be negligible for this event. At the time of the March 96 storm event the oak-hickory vegetation on the hillslope was not yet in leaf. We therefore assumed that ET was relatively small on the event scale compared to other components of the water balance. There was also no experimental data available to estimate hillslope-specific potential ET or to validate the simulated actual ET. The upslope boundary and the sides of the domain were treated as no flux boundaries. Two boundary conditions were defined at the downslope boundary of the hillslope. A seepage face boundary condition was assigned to the soil sublayer across the entire width of the domain, allowing water to leave the domain through the saturated part of the boundary. The code assumes a pressure head equal to zero along the saturated part of a seepage face boundary. The subsurface flow that is reported in the following text, however, originates only from the nodes that correspond to the location of the 20 m wide trench at the field site (see black bar in Fig. 1b). The bedrock sublayer was assumed to have no flux at the downslope boundary, implying that flow in the bedrock is primarily vertical and that lateral flow within the bedrock can be neglected. A free drainage boundary condition was specified for the bottom boundary (the bedrock), assuming a unit total vertical hydraulic gradient (i.e. a zero pressure head gradient). Initial conditions were defined in the pressure head by assuming a pressure head of −0.7 m everywhere in the domain followed by a 7 day drainage period without atmospheric input prior to the start of the actual rainstorm. This corresponded to actual field conditions where the 6–7 March 1996 storm was preceded by a 7-day dry period and subsurface runoff had stopped and pressure heads were almost at steady-state prior to the onset of the storm event. The total simulation time was 15 days.

During calibration of the van Genuchten parameters α and n, outflow from the nodes along the seepage face that corresponded to the location of the trench in the field was compared to the subsurface stormflow that was collected at the ten 2 m trench sections of the study hillslope as a response to the rainstorm (excluding flow from the soil pipes). Model performance was evaluated by calculating the Nash–Sutcliffe efficiency (NSE):

$$NSE = 1 - \frac{\sum_{t=1}^{n}(P_t - O_t)^2}{\sum_{t=1}^{n}(O_t - \bar{O})^2}$$

where P_t are the modeled values, O_t are the observed values, n is the number of measurements, and $\bar{O}$ is the mean of the observed values. The efficiency statistic ranges between 1 and $-\infty$, with 1 indicating a perfect match between observed and modeled values and NSE less than zero indicating that the mean of observations is a better predictor for O_t than the model.

After the calibration, the base case parameterization was tested against tensiometer readings. Time series of pressure heads at the locations within the model domain that corresponded approximately to the location of the field tensiometers were compared to field observations. Model performance was again evaluated by calculating the NSE.

Variation of controlling factors

Using the base case described above, we used the model to explore the interplay between four controlling factors (i.e. hillslope variables): bedrock permeability (defined here as the contrast between soil and bedrock saturated hydraulic conductivities), slope angle, soil depth and storm size. We systematically varied each of these obtaining 72 combinations of our chosen hillslope variables (Table 2).

So why these particular four factors? Storm size was selected based on previous process-based work at the site that has shown clearly that rainfall amount is the single most important determinant of subsurface flow initiation and production (Freer et al., 2002; Tromp-van Meerveld and McDonnell, 2006a). The storm size was varied by scaling down the hourly precipitation records by one third to 58 mm (storm return period: ~6 months) and by two thirds to 29 mm (storm return period: ~4 weeks), keeping the temporal dynamics of the intensities unchanged. The storm sizes we tested were thus guided by the known threshold rainfall amount of approximately 55 mm necessary for flow generation in the base case (Tromp-van Meerveld and McDonnell, 2006a) and at the upper end, by the amount of rainfall necessary to induce overland flow at the surface. Thus, we restricted our simulations to those producing subsurface flow only. Field monitoring at the Panola hillslope since the mid-1990s (McDonnell et al., 1996) has failed to detect any overland flow – either from infiltration excess or saturation excess. The infiltration capacity of the sandy loam soil appears to be greater than all but the most extreme rainfall intensity return periods. Similarly, the apparent hillslope-scale anisotropy in soil hydraulic conductivity is such that water tables, even though they develop within the soil profile in a transient manner, rarely exceed 0.5 times the soil depth (Tromp-van Meerveld and McDonnell, 2006b). Admittedly, Hydrus-3D is not able to simulate overland flow; but we do not consider this a constraint given these field realities. Slope angle was selected as another controlling factor for our virtual experiments. Slope angle has been shown at Panola and elsewhere to be a key factor for defining the hydraulic gradients necessary to drive subsurface flow. Our range of slope angles used in the experiments here covers the range of slopes from various other field sites that have reported subsurface stormflow initiation (reviewed recently by Weiler et al., 2005). The slope angle of the domain was decreased to 6.5° and increased to 26° and

Table 2
List of controlling factors (i.e. hillslope variables) that were varied in the virtual experiments and their tested levels.

Controlling factor	Low	Medium	High	Very high
Mean soil depth (m)	0.6[a]	1.2	1.8	–
Difference K_s soil–bedrock	10^1	10^{2a}	–	–
Slope angle (°)	6.5	13[a]	26	40
Storm size (mm)	29	58	87[a]	–

[a] Combination of controlling factors that is present at the Panola study hillslope including the original observed storm.

40°. Bedrock permeability was isolated as another controlling factor. Again, this selection derived from field data and field experiments at Panola and elsewhere. Tromp-van Meerveld et al. (2007) showed that due to permeable bedrock vertical leakage into bedrock is a major component of the hillslope water balance. Here again, we restricted our ranges for bedrock permeability to limit the occurrence of overland flow. The saturated hydraulic conductivity K_s of the two bedrock layers was increased by one order of magnitude, thus reducing the conductivity contrast between soil and bedrock. Finally, soil depth was selected as a factor in our analysis. Numerous studies on experimental slopes have defined soil depth as a key factor for storage and re-distribution of storm rainfall and important filter between rainfall input and lateral flow generation (Lin, 2006). Because soil depths at some points in the domain were already very shallow, the soil depth was only increased by adding 0.6 m and 1.2 m, respectively, to the soil sublayer.

We focused in our virtual experiments on three of the more important physical hillslope attributes influencing subsurface stormflow generation that cannot be investigated separately in the field at one site. The only variable external driver examined was storm size. Antecedent moisture conditions could have been another important controlling factor to consider. However, we chose storm size over antecedent moisture conditions because previous field work at the Panola study hillslope had suggested that storm size was of greater importance for the generation of subsurface stormflow than antecedent moisture conditions (Tromp-van Meerveld and McDonnell, 2006a).

Additional simulations were run with a spatially uniform soil depth (0.6 m) overlying the bedrock topography for the four tested slope angles. In these cases, the surface topography mimicked the bedrock topography. These exploratory simulations allowed comparing the effect of spatially variable soil depth and of spatially uniform soil depth distribution while keeping the total soil volume constant and helped better understand the importance of the soil mantle for the hydrologic response.

The results were analyzed against a number of common metrics of hillslope hydrologic response (Mosley, 1979): runoff coefficient (total subsurface stormflow/total input), time from onset of storm to onset of subsurface stormflow (response time), duration of subsurface stormflow, time to peak and peak discharge. Also the spatial variability of subsurface stormflow along the 20 m trench was considered by dividing the model seepage face boundary into 10 sections, each 2 m wide, and calculating contributions from these individual sections. This corresponds to the way subsurface stormflow is collected at the Panola study hillslope.

Using a 3D model allowed us to follow the temporal and spatial dynamics of internal state variables through the event. In order to better understand results of the virtual experiments, spatial patterns of subsurface moisture and flow velocities were analyzed.

Computational times for each simulation ranged between 10 min and 11 h, depending on the size of the domain, the extent of the development of saturated areas within the model domain and the occurrence of outflow at the seepage face boundary. The quality of the simulations was checked against mass balance errors. No numerical instabilities were encountered.

Digital terrain analysis

The digital terrain analysis (DTA) was performed for the bedrock topography of the four tested slope angles and is independent of the thickness of the overlying soil mantle. The importance of the topography of the underlying impeding layer ("bedrock") for the generation and routing of subsurface stormflow has been recognized in the past 15 years (McDonnell et al., 1996). Groundwater flow in a traditional sense is primarily gradient-driven. The saturated subsurface flow that we are investigating in this study, however, is a shallow ribbon of mobile water flowing in the saturated domain along the soil–bedrock interface. In this case, downslope microtopographic impediments in the subsurface can be a barrier for flow, interrupting and/or redirecting flow. Freer et al. (2002) showed for the Panola study hillslope that the observed spatial distribution of subsurface stormflow could be very well explained with the flow accumulating characteristics of the bedrock surface. We therefore based our topographic analysis on the bedrock topography, not the topography of the soil surface. Two topographic indices were used in the DTA, taking upslope as well as downslope topography into account. Flow accumulation (FA) for each cell was calculated from the 1 m DEM interpolated from the surveyed 2 m grid using the single-flow-direction D8 algorithm (Jenson and Domingue, 1988). The FA algorithm determines the number of cells upslope that drain into the respective cell, i.e. the upslope contributing area of each cell. On the catchment and watershed scale, FA is often used to identify stream channels and areas of stream initiation. In this study, we used it to delineate flow paths and to identify areas where water is collected.

The downslope index (DI) is a measure for the downslope drainage efficiency of a location (Hjerdt et al., 2004). It is defined as the horizontal distance one has to go in downslope direction (following the steepest-direction flow path) to descend a predefined vertical distance. We used the DI to determine the drainage properties of each cell. A long horizontal distance indicated that drainage from that cell was slow and less efficient. Potential fill areas, i.e. areas where water was collected and retained, were defined as locations with a FA $\geqslant$ 10 cells and a DI > 3 m. Spill areas, i.e. areas that accumulated water and efficiently drained this water further downslope, were defined as locations with FA $\geqslant$ 10 cells and DI $\leqslant$ 3 m.

Results and discussion

Calibration and testing of the base case

The first half of the 87 mm bimodal rainstorm event did not induce significant subsurface stormflow at the study hillslope trench face (Fig. 1a). Approximately 3 h after the start of the second half of the rainstorm, subsurface stormflow sharply increased, peaking 7 h later, coincident with the stoppage of rainfall. The measured hydrograph was characterized by a double peak with a secondary plateau-like peak occurring approximately 6.5 h after the storm rainfall had ceased. Total subsurface stormflow (flow from the ten 2 m sections only, excluding flow collected from the soil pipes) measured at the trench as response to the rainstorm event was 13.5 m³ (corresponding to a runoff coefficient of 11%) with a peak discharge of Q_{max} = 0.84 m³ h⁻¹.

The simulated subsurface stormflow hydrograph was consistent with many of the measured spatial and temporal features of the field subsurface stormflow hydrograph (Fig. 1a) and also the other hydrological parameters that we evaluated it against. Modeled subsurface stormflow was initiated only in the second half of the bimodal storm event. The simulated hydrograph also showed a double peak and a secondary peak 6 h after the end of the input. The modeled recession was somewhat slower than measured values. Subsurface stormflow stopped after 5.8 days. Total simulated subsurface stormflow was 14.3 m³ (runoff coefficient of 12%) with a peak discharge of Q_{max} = 0.62 m³ h⁻¹. The Nash–Sutcliffe efficiency was 0.86, indicating a good overall model performance. These results also indicated that it was acceptable for the simulated event to not include soil pipes in the model. For the simulation of longer time series, however, we would expect that the explicit representation of the soil pipes would become necessary. The entire flux that was reported for the seepage face boundary ex-

ited the model domain at the lowermost soil layer. This corresponded very well with field observations.

More important than a perfect match to trench flow alone was the model's ability to capture both the integrated trench outflow and the internal spatially distributed pressure head dynamics as measured in the field. Fig. 1c shows the results of the testing of the model against tensiometer readings. Nash–Sutcliffe efficiencies ranged between 0.87 (tensiometer 3) and −1 (tensiometer 6), indicating that at some locations, the model performance with respect to pressure head simulation was quite good while at other locations, the model did not match the observations very well. In some instances, the field data indicated saturation (positive pressure heads) where the model results did not (e.g. tensiometer 6) and vice versa (e.g. tensiometer 2) which would suggest that observed and simulated saturation patterns were different. In the model HYDRUS-3D, observation points were defined in mesh nodes. Due to the arrangement of nodes in mesh layers, there was not always a node at exactly the required depth to match the tensiometer cups. This resulted in deviations from the reported field installation depths ranging between 0.8 and 8.5 cm that were able to explain the differences in observed and simulated pressure heads mentioned above. Even if the comparison of absolute values showed some disagreement in some cases, the model (that was parameterized based on trench outflow) predicted the timing and also amplitude of pressure head changes in general very well, confirming that the base case scenario captured the major internal flow behavior. This is significant because field-based work and theoretical study of the Panola hillslope have shown that connectivity of patches of positive pore pressure are the pre-condition for flow generation at the trench face. These simulations were consistent with the mechanistic behavior at the site and thus assumed to be a solid foundation for our exploration of interactions of altered variables.

It was interesting to note that the homogeneous model parameterization that was based on an integrated flow characteristic, i.e. trench discharge, was at the same time able to reproduce spatially distributed pressure head values. This seemed to suggest that it was not necessary to explicitly describe soil pipes and other soil heterogeneities to reproduce the behavior of "point" quantities during the storm.

Additionally, the precipitation threshold of the base case scenario for the initiation of subsurface stormflow was tested (under constant initial conditions) by reducing the original storm size in a stepwise fashion (by 10% each step down to 30% of the original storm). When we used the same 1 mm runoff threshold for defining "significant subsurface stormflow" as per Tromp-van Meerveld and McDonnell (2006a), the base case scenario produced significant subsurface stormflow only when the input exceeded approx. 54 mm (results not shown). This value agreed very well with the reported precipitation threshold of 55 mm necessary for flow activation.

Virtual experiments: effects of hillslope variables on hydrologic response

Virtual experiments were performed across the range of factor combinations listed in Table 2. No substantial subsurface stormflow (<1 mm) was observed if the contrast between K_s of soil and bedrock was equal to 10^1. This difference in hydraulic conductivities did not seem to be sufficient under tested conditions to generate lateral subsurface flow. Therefore, there are no further results for half of the simulations where the K_s-contrast was equal to 10^1. Results were summarized using "response surfaces" for each hillslope metric. Fig. 2 shows examples of response surfaces. Although the visualized interpolation implies that the combination space of controlling factors was continuously sampled, only 12 discrete combinations per storm size were simulated (as shown by the labeling of the axes – 4 slope angles, 3 soil depths). Therefore, we should note that the interpolation between sampling points is an assumption and does not necessarily reflect the behavior of combinations not tested. The response surfaces in Fig. 2 show the types of interplay between factors: a primarily horizontal or vertical color gradient indicates that one controlling factor dominates the response (Fig. 2a); a more diagonal gradient (as in the case of Fig. 2b) suggests that both factors similarly influence the re-
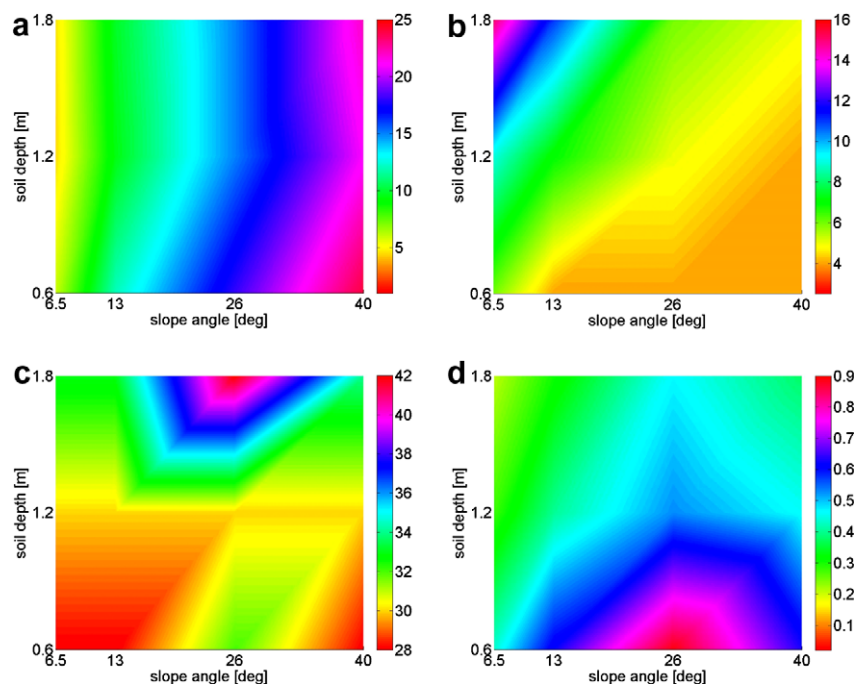

Fig. 2. Response surfaces visualizing the types of interplay between slope angle and soil depth for the 87 mm storm scenarios for selected hydrologic metrics: (a) subsurface runoff coefficient (m³ m⁻³), (b) response time (h), (c) time to peak (h) and (d) peak discharge (m³ h⁻¹).

sponse without interaction; and a pattern without clear gradient in one direction (none of the above) indicates complex or non-intuitive interaction between the controlling factors (Fig. 2c and d). Here we define interaction such where the effect of one predictor on a response variable depends on the value of another predictor.

Analysis of all the possible response surfaces (see Fig. S2 in the Supplementary information) indicated that the initiation of significant (>1 mm) subsurface flow was controlled by storm size as well as slope angle. The small storm induced subsurface stormflow only on the 40° slope; the medium-sized storm did not induce flow on the 6.5° slope. Our results suggest that slope angle dominated the subsurface stormflow runoff coefficient, i.e. the steeper the hillslope, the higher the cumulative subsurface stormflow (Fig. 2a). The response time increased with soil depth and decreased with slope angle, showing a superposition of effects (Fig. 2b). The duration of subsurface stormflow was controlled mainly by the slope angle. Time to peak became shorter with increasing storm size and was also strongly influenced by soil depth, but not appreciably affected by slope angle. In the combination between the 26° slope and the largest storm, however, time to peak was significantly longer for the shallow and the deep soil than at all other slope angles, but not for the intermediate soil depth, suggestive of some complex interactions between soil depth and slope angle (Fig. 2c).

The behavior for peak discharge was less intuitive (which we later analyze in our connectivity analysis section). For the medium size storm, peak discharge was clearly influenced by slope angle and also by soil depth; particularly going from the shallow to the intermediate soil depth. In combination with the largest storm size, however, peak discharge increased as the slope angle increased from 6.5° to 26° but decreased considerably again in the 40° scenarios (Fig. 2d). This behavior was observed for all three tested soil depths. With increasing soil depth peak discharge values decreased. The spatial variability of subsurface stormflow was strongly reduced with increasing storm size and as the hillslope became steeper and increased slightly with increasing soil depth. Comparing the color palettes between storm sizes showed that rain amount generally had an intensifying effect on the hydrologic response. Additionally, the occurrence of complex interactions between controlling factors was governed by rain amount; i.e. complex behavior was only found in combinations with the largest storm (see Fig. S2 in the Supplementary information).

Hydrograph response also varied spatially across the trench face. Fig. 3 shows as an example the distribution of subsurface stormflow along the trench plotted as cumulative subsurface stormflow simulated for each of the individual 2 m trench sections
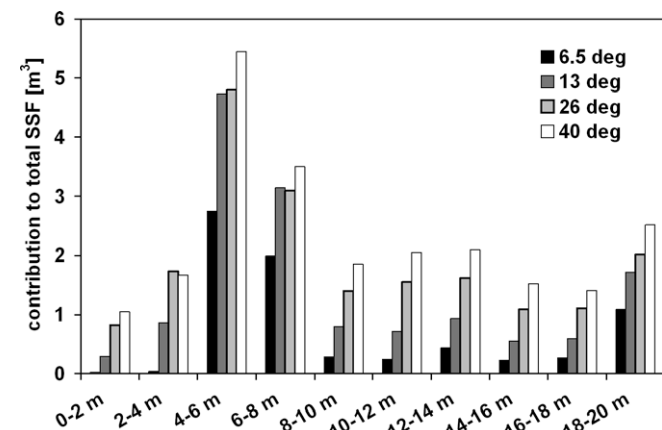
for the slope angle variations of the base case (0.6 m soil depth, 87 mm storm). The highest flow contributions were always obtained at the trench sections 4–6 m, 6–8 m and 18–20 m (measured from the left). Some sections contributed minimally to flow at 6.5° but then showed a strong increase in subsurface stormflow at higher slope angles whereas for other sections the subsurface stormflow did not change as dramatically. Fig. 3 also demonstrates the decreasing variability of spatial distribution of subsurface stormflow along the trench with increasing slope angle.

Connectivity analysis

Significant lateral subsurface stormflow only occurred when more or less well connected hillslope-scale areas of saturation or near saturation (within 95% relative saturation) developed at the soil–bedrock interface (Fig. 4). This is consistent with previous field observations at the site where significant subsurface stormflow response is observed only when saturation develops at the soil–bedrock interface and these saturated areas connect across the slope and become linked to the trench face (Tromp-van Meerveld and McDonnell, 2006b).

The most obvious control on the formation of larger-scale saturation or near-saturation was bedrock permeability. Fig. 4 shows a visualization of the relative saturation at the soil–bedrock interface for the slope angle variations of the base case and the corresponding scenarios with the higher bedrock hydraulic conductivity for one time step (2 h before the end of the event). The images suggest that a minimum contrast in hydraulic conductivities between the conductive and the impeding layer was needed to enable the ponding of water and to initiate subsurface stormflow. Fig. 4 also demonstrates that near-saturation was also a sufficient condition for the initiation of fast subsurface stormflow (dependent on the slope angle) as long as those areas were connected to each other and the downslope boundary. The occurrence, the extent of, and the ratio between saturated and near-saturated areas were also influenced by the other tested hillslope variables which we now explore in detail below.

Slope angle effects on connectivity

Slope angle generally had an intensifying effect on the hydrologic response of the hillslope due to the increasing elevational gradients with increasing slope angle (Fig. 2). Quite unexpectedly, however, in conjunction with the largest storm peak discharge values – as opposed to the runoff coefficient – did not increase consistently with increasing slope angle (Fig. 2d). This inconsistent behavior was observed at all tested soil depths, indicating that it was particularly related to slope angle effects. Notwithstanding the low peak discharge values at 40°, total subsurface stormflow was still highest at this slope angle because the high elevation gradients led to an early start of subsurface stormflow, continuous flow throughout both halves of the event and an overall long subsurface stormflow duration. To explain this effect of the slope angle on the hydrologic response, we needed to better understand the topographic controls on subsurface stormflow.

Our digital terrain analysis (DTA) of the bedrock surface showed that at 6.5°, a few individual flow paths with higher flow accumulation (FA) could be identified upslope (Fig. 5). However, there did not seem to be a continuous flow path connecting upslope areas to the trench. At 13° (the scenario using the original Panola DEM), distinct flow paths were identified, that were connected to the trench. The FA map indicated a strong concentration of flow from larger upslope areas into a few downslope cells. The identified flow paths joined together downslope and were concentrated into a narrow section on the left side of the trench. At 26°, flow concentration was still discernible from diagonally running lines with higher flow accumulation but at the same time more parallel running flow
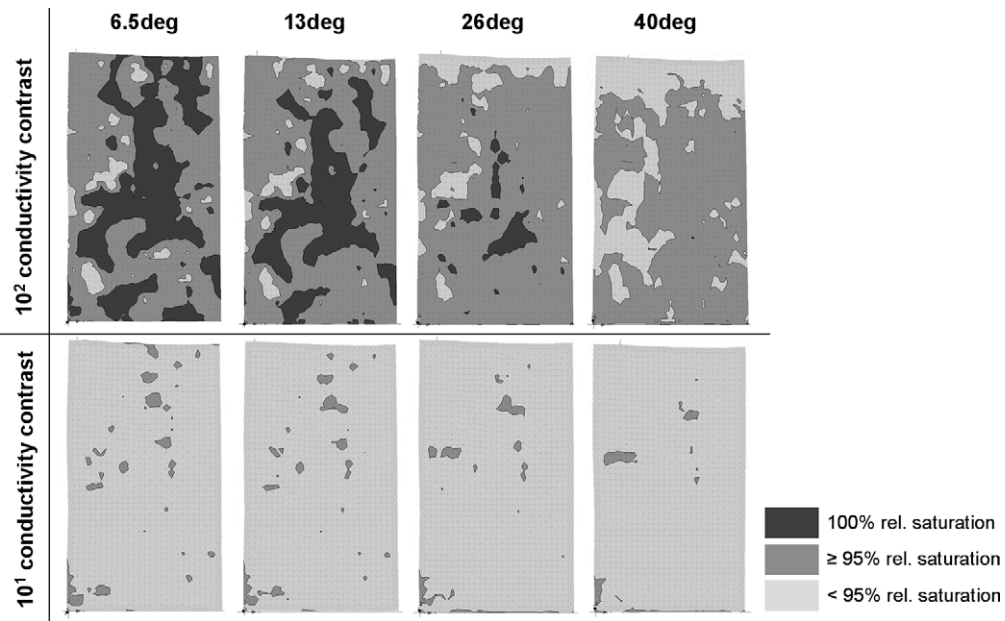

Fig. 3. Cumulative subsurface flow for individual 2 m sections of the slope angle variations of the base case scenario (soil depth 0.6 m, 87 mm storm).

Fig. 4. Effect of bedrock permeability on the formation of saturation at the soil–bedrock interface (soil–bedrock interface). Patterns of saturation (2 h before the end of the event) at the soil–bedrock interface for the bedrock K_s variations of the base case scenario (soil depth 0.6 m, 87 mm storm).
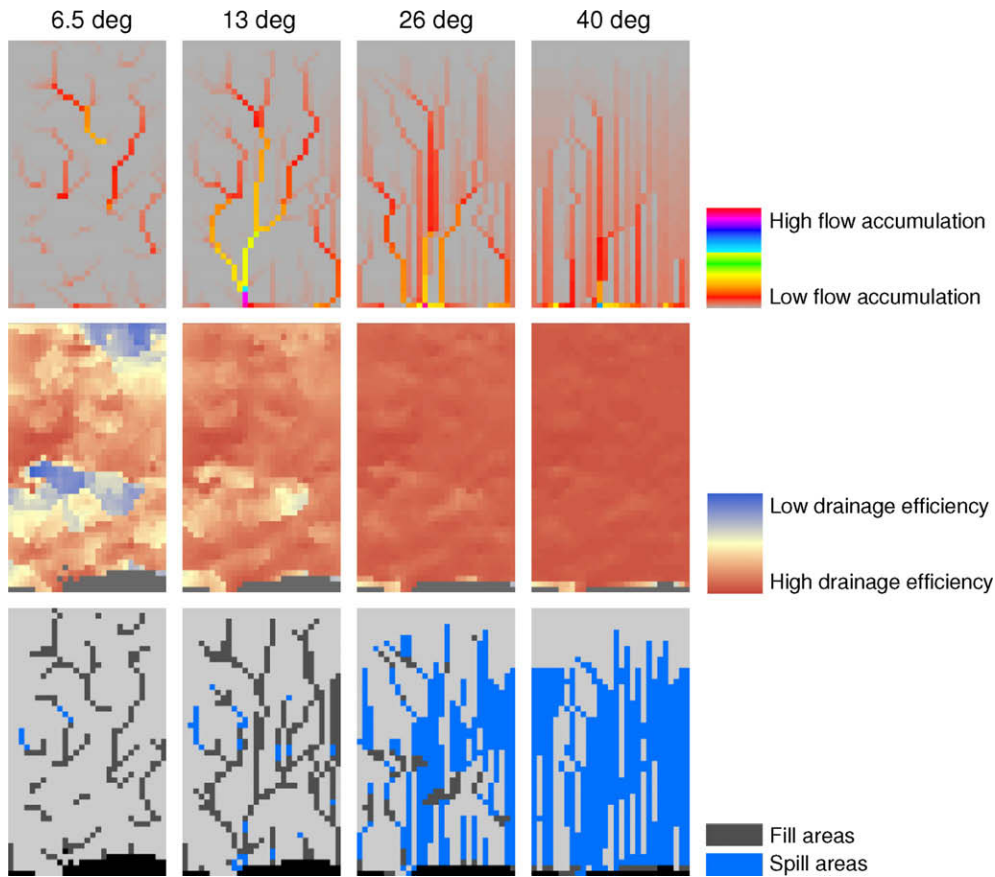

Fig. 5. Digital terrain analysis. Maps of flow accumulation (top), downslope index (middle) and fill and spill areas (bottom) for the four tested slope angles.

paths, normal to the trench, appeared and FA was distributed more uniformly across the downslope boundary. At 40°, the FA map indicated that the flow concentration effect had considerably weakened; flow paths were mainly parallel and normal to the trench. The maps showing the downslope index (DI) for the four slope angles indicate that in the 6.5° and 13° cases, extended areas with less efficient drainage existed. The distribution of the DI clearly reflected the topography (see Fig. 1b), with topographic depressions and flatter areas having a high DI, i.e. low drainage efficiency. The overall drainage efficiency increased with increasing slope.

Combining flow accumulation and drainage efficiency showed how the balance between fill and spill explains some of the interactions between slope angle and peak discharge. At 6.5°, many isolated fill areas were identified across the hillslope but hardly any spill areas. At 13°, even more fill areas were present, often stretching continuously along and across the hillslope. However, fill areas were very well connected to each other and to the trench by spill areas. This implied that once the fill areas spill – when precipitation exceeds the threshold dictated by topographic impedance – the released water can efficiently be routed downslope at this slope angle. At 26°, fill areas were still present in the upslope and midslope sections but extensive spill areas dominated the bedrock surface. At 40°, no fill areas (other than those in immediate proximity of the trench) were identified. These results suggested that as slope angle increased, the system transitioned from a fill-dominated regime (at 6.5°) to a fill and spill regime (at 13 and 26°) and then to a spill-dominated system (at 40°).

Whilst our DTA does not explicitly quantify bedrock depression volumes, we hypothesize that by increasing the slope angle, the volume of bedrock pools and the height of spilling barriers will decrease, thereby changing the balance between fill and spill and thus the timing and spatial distribution of water flow on the hillslope. As a result, the precipitation threshold would be expected to change. This is consistent with our model findings where the initiation of significant subsurface stormflow was controlled by the slope angle. The dominance of filling at 6.5° was reflected in the largest areal extent of saturated area at the soil–bedrock interface (Fig. 4) and the highest rise of transient water tables into the soil profile. Saturation at the soil–bedrock interface persisted longest at this shallow slope angle (see Fig. S3 in the Supplementary information). Although large-scale connected patterns of saturation developed on up- and midslope areas during the event, they did not connect to the downslope boundary (as was the case, e.g. for the 13° scenario). This behavior reflected very well the missing connection of fill areas to each other and downslope areas by spill areas that was identified with the DTA. As a result, the 6.5° slope produced only a small trench response (in combination with all tested soil depths and storm sizes, compared to the other tested slope angles) and, at the same time, the highest loss of soil moisture to the underlying bedrock. As the slope angle was increased and the topography control shifted to a fill-and-spill regime (at 13 and 26°) and then to a spill-dominated regime (at 40°), the total subsurface stormflow response at the trench increased. The spill-dominated regime at 40° led to an early start of subsurface stormflow, continuous flow throughout both halves of the event and a long duration of subsurface stormflow. This suggested that fill areas lead to a delayed response and that they are potential areas for flow interruption. Fill areas produce a threshold and need a certain input before the water accumulated in the fill areas can spill over the bedrock ridges (spill barriers) and flow downslope. Consequently, scenarios that are characterized by a balance between fill and spill, like the 13° and the 26° scenarios, will produce an interplay between the retention of water in fill areas and – once a topography-specific threshold is exceeded – a sudden release of water. Particularly at 26°, where in the upper portions of the hillslope spill areas, i.e. flow accumulating areas with high drainage efficiency, were located upslope of fill areas, ensuring an efficient accumulation of water in fill areas, the topography had the potential for strong sudden responses. Depending on topography (slope angle and bedrock microtopography) this can happen at a few areas at a time or in a more synchronized way across the hillslope, leading to an intensified response further downslope. Analysis of the peak times of the individual 2 m sections for the slope angle variations of the base case (see Table S1 in the Supplementary
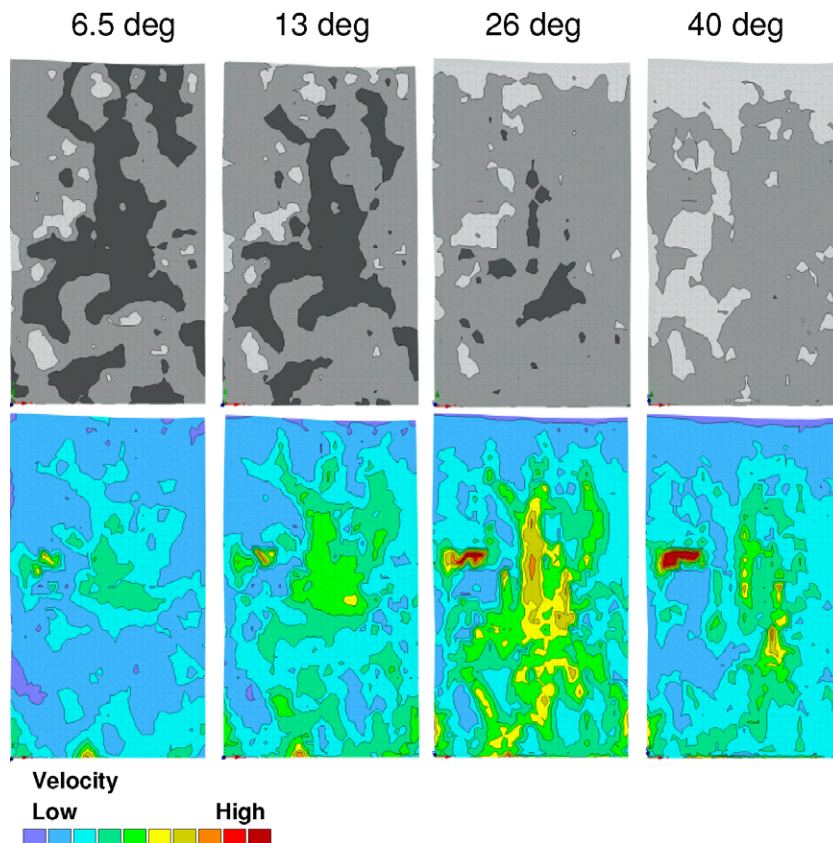

Fig. 6. Patterns of relative saturation (color scale is as Fig. 4) and corresponding velocities 2 h before the end of the event for slope angle variations of the base case scenarios.

information) revealed that in the scenarios that were characterized by a balance between fill and spill, i.e. at 13° and 26°, peak times were more variable than in the other cases. At 13°, the two sections between 4 and 8 m peaked 7–8 h later than the rest. These sections had the highest flow accumulation, with flow paths extending far upslope and comprising fill as well as spill areas. At 26° six sections peaked late, causing the unexpectedly late overall peak, and again those were the sections that had long flow paths connecting the upslope and midslope fill areas to the downslope boundary. These findings pointed at the importance of the timing of water flow as a result of fill and spill processes on the hillslope.

Finally, returning to the interaction between peak discharge, slope angle and storm size, we compared the fill and spill maps with time snapshots of the simulated patterns of moisture dynamics at the soil–bedrock interface (Fig. 6). These comparisons suggested that patterns of saturation approximately mimicked the shape of the fill areas, i.e. that 100% relative saturation occurred primarily in fill areas. No fill areas were identified at the 40° case, and therefore no transient water tables could develop. Adding the corresponding patterns of flow velocities to the comparison showed that higher velocities were reached in saturated or near-saturated areas (Fig. 6). Apart from the location of the rocky outcrop (center left side) with steep local slopes in the bedrock topography, highest flow velocities were generally observed in spill locations. Flow vector maps (see Fig. S4a–d in the Supplementary information) reflected very well the flow paths identified in the FA maps, consistent with Tromp-van Meerveld and McDonnell's (2006a) hypothesis that lateral subsurface flow occurs along the soil–bedrock interface, i.e. parallel to the bedrock surface, and is restricted to topographic lows. The weak connection between mid- and upslope areas and the trench in the 6.5° scenario was also reflected by the flow velocities; no continuous path with higher flow velocities developed in this scenario. At 26°, the combination of steeper slopes and the (still) existent fill areas led to a particularly pronounced and synchronized fill and spill reaction, causing a concentrated downslope movement of water with high flow velocities (as visible in Fig. 6). Although the hydraulic gradient was increasingly controlled by the elevational potential as the slope angle was increased, higher flow velocities could not develop on the 40° slope because without fill areas, no saturation could form. Therefore, no sudden releases of water occurred and therefore flow remained unsaturated. As a consequence, peak discharge values were lower than at 26°. The observed unexpected and (at first) non-intuitive behavior with respect to peak discharge was a result of an interaction – in this case how the combination of bedrock topography and slope angle shaped the fill and spill mechanism and controlled the temporal and spatial distribution of water across the hillslope and resulting flow velocities.

Soil depth effects on connectivity

Increases in soil depth led to a general attenuation of the hillslope hydrologic response (Fig. 2). The subsurface stormflow started later, the time to peak increased and peak discharge values decreased. Of course in deeper soils, the vertical travel distance of the input signal from the soil surface to the impeding layer at the soil–bedrock interface (where the diversion to lateral flow occurred) was longer. Therefore the build-up of saturation and the initiation of subsurface stormflow were later. Deeper soils also have more total storage volume and modulate incoming precipitation peaks more effectively, thereby damping the response. Interestingly, runoff coefficients were not greatly affected by soil depth changes although the extent of saturated area at the soil–bedrock interface decreased considerably with increasing soil depth (see Fig. 8). This indicated that soil depth affected the hydrologic response in both time and space.

So how does soil depth affect the formation of saturation at the soil–bedrock interface and whole hillslope connectivity? Fig. 7 compares the soil depth map with the development of saturation at the soil–bedrock interface for the base case scenario. The comparison revealed that moisture content rose first in areas with shallow soil, as proposed by Tromp-van Meerveld and McDonnell (2006b). In these areas the travel distance for the input signal down to the impeding layer was short causing an early ponding of water. These areas, however, were not the areas where 100% relative saturation, i.e. transient water tables, formed (Fig. 7). In the course of the event, water was redistributed and routed along the topographic lows of the bedrock surface into bedrock depressions, i.e. the fill areas. Bedrock depressions tended to have deeper soils. This was also indicated by the relatively planar ground surface overlying the irregular bedrock topography. Therefore, patterns of relative saturation reflected to some extent the soil depth distribution, especially at the lower slope angles.

The comparison of the moisture dynamics at the soil–bedrock interface for the three soil depths (applies to all tested slope angles) showed that soil depth affected the size of saturated or near-saturated patches and the connectivity between those patches and to the downslope boundary (Fig. 8). The degree of connectivity determined the length of the effective flow paths, and as described above, highest flow velocities were reached in saturated areas. Less connectivity resulted in lower overall flow velocities and a slower response with deeper soils. The fill and spill mechanism as shaped by the slope angle and bedrock topography and
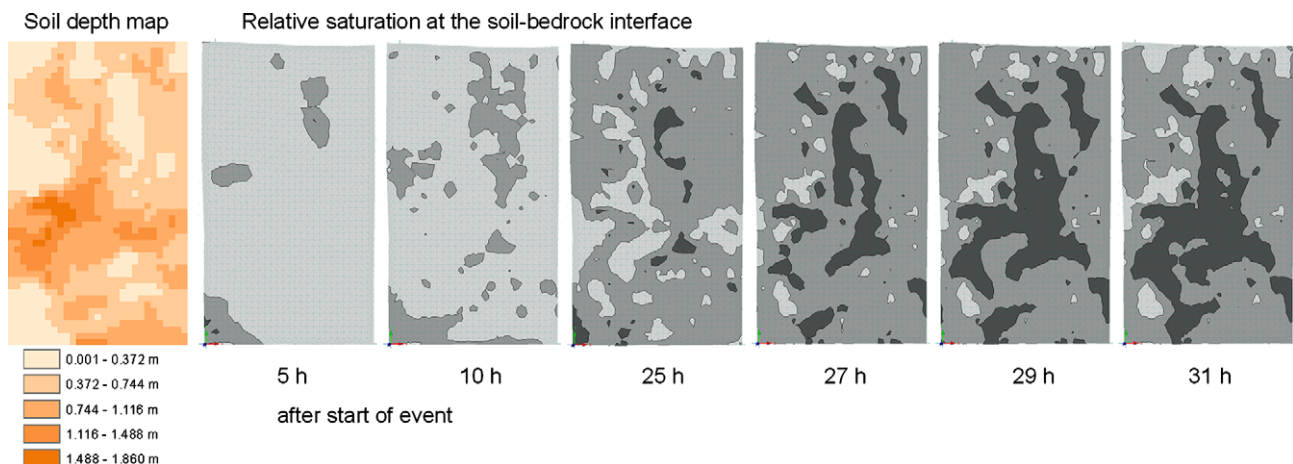

Fig. 7. Soil depth map and development of relative saturation at soil–bedrock interface for the base case scenario for six time steps (times in hours after start of event; event ends at 31 h). Color scale for relative saturation is as Fig. 4.
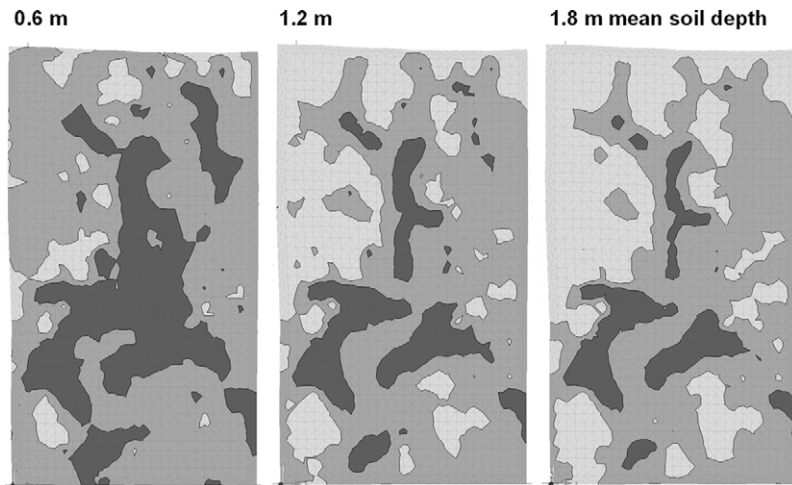
0.6 m   1.2 m   1.8 m mean soil depth

Fig. 8. Influence of soil depth on connectivity of saturation at soil–bedrock interface. Patterns of relative saturation at the end of the storm for the soil depth variations of the base case scenario (13° slope and 87 mm storm) for 0.6 m mean soil depth (left), 1.2 mean soil depth (middle) and 1.8 m mean soil depth (right).

the effect of the slope angle on the hydraulic gradient in general still led to similar subsurface runoff coefficients.

Additional simulations with uniform soil depth (0.6 m) on the four tested slope angles were run to explore the interaction between soil depth distribution and slope angle. Most results of our simulations with uniform soil depth across the hillslope were similar to the results found for the variable soil depth distribution (see Fig. S5 in the Supplementary information). With increasing slope angle, the runoff coefficient increased, the response time and the spatial variability of subsurface stormflow decreased. Peak discharge again increased from 6.5° to 26° but was significantly lower at 40°, indicating that the general interplay between the fill and spill mechanism and the slope angle were not greatly affected by the explicit distributions of soil depth. Time to peak did not differ significantly, suggesting that this metric was controlled by the total soil volume rather than actual soil depth distribution.

Interactions between slope angle, soil depth and storm size were found in combinations of the 26° slope and the biggest storm (see Fig. 2c). An analysis of the peak times of the individual 2 m trench sections of these particular scenarios showed that for both the shallow and deep soil scenarios, six sections peaked late leading to the delayed overall peak in those scenarios and the emergence of complex interactions (see Table S2 in the Supplementary information). For the 0.6 m soil, the sections from 2–14 m peaked 3–4 h later than at other tested slope angles; for the 1.8 m soil, the sections from 0 to 12 m reached peak discharge approx. 8–9 h later. This trend was not found in the case of the intermediate soil depth (1.2 m); here, only three sections (2–8 m) peaked approx. 8 h later, producing a hydrograph that resembled the ones found for other slope angles. The interaction found for time to peak with variable soil depth (Fig. 2c), however, was not seen in the simulations with uniform soil depth, clearly showing that this interaction was a result of the interplay between subsurface topographic control and the overlying soil mantle and its particular distribution of soil depth. The soil mantle and the soil depth distribution controlled the travel times of the input signal to the soil–bedrock interface and determined when and where the ponding of water started and, hence, the timing of connectivity, particularly in relation to the still ongoing event.

Storm size effects on connectivity

Three of our tested hillslope variables (bedrock permeability, slope angle and soil depth) can be considered rather fixed at a given field site (at least over our common monitoring time frame).

Thus, we might classify them as part of the "hillslope configuration". Storm size, in contrast, is a temporally variable factor, much like antecedent moisture conditions or evapotranspiration. Fig. 9 shows an example of the saturation patterns that developed on the same hillslope configuration as response to the three tested storm sizes. These data suggest that the ponding of water at the soil–bedrock interface as well as the degree of connectivity were also controlled by the size of the input (rates as well as the total amount). The input must be large enough to overcome bedrock microtopographic detention storage and leakage rate to deeper layers. In our analysis, each case that did not produce significant subsurface stormflow (despite the larger contrast in hydraulic conductivities between soil and bedrock) showed that the input was too low to allow for substantial ponding of water at the soil–bedrock interface. With smaller storms, patches of saturation (or near-saturation) were smaller and the degree of connectivity was markedly lower resulting in lower flow velocities and smaller trench responses. Overall these results suggest that for the generation of significant lateral subsurface stormflow along the soil–bedrock interface, the input must exceed the topography-related threshold to induce spilling that leads to connection. Depending on antecedent moisture conditions, this will most likely require varying event sizes although, in the case of the Panola study hillslope, experimental data suggest that storm size trumps antecedent moisture conditions in its influence on subsurface stormflow (Tromp-van Meerveld and McDonnell, 2006a). If the event is too small to induce pronounced filling and spilling reactions across the hillslope, there will be no sudden release of water. Those sudden release reactions, however, generate sizeable amounts of subsurface stormflow, causing the non-linear relationship between rainfall and subsurface runoff. This appears to be the reason why interactions and unexpected behavior were only found in combination with the biggest storm. Without spilling, the presence of fill areas had an impeding effect, resulting in the interruption of flow. Consequently, the elevational component of the hydraulic gradient created by the slope angle dominated the hydrologic response. Thus, in combination with the medium storm size, peak discharge increased consistently with increasing slope angle (see Fig. S2 in the Supplementary information).

A conceptual model of the hillslope interactions and connectivity

So how might we conceptualize the various controls and interactions revealed through our virtual experiments and visualiza-
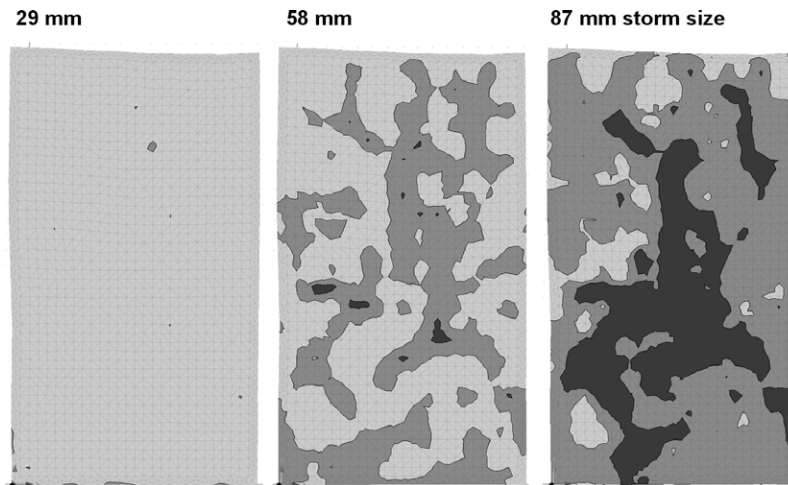
Fig. 9. Influence of storm size on connectivity of saturation at soil–bedrock interface. Pressure head distribution at the end of the storm for base case hillslope configuration (13° slope and 0.6 m mean soil depth) for 29 mm storm (left), 58 mm storm (middle) and 87 mm storm (right).

tions? Clearly, our interpretation needs to be consistent with the field work of Tromp-van Meerveld and McDonnell (2006a) who showed that the precipitation threshold at the Panola study hillslope necessary for the initiation of significant subsurface stormflow was approx. 55 mm. The base case model domain used in our virtual experiments was able to reproduce this rainfall threshold and also to represent the same fill and spill behavior as noted by Tromp-van Meerveld and McDonnell (2006b) as a mechanistic explanation of the observed whole-slope response. Going beyond the single-realization experimental hillslope, our findings with the model illustrated that the internal response and the trench outflow were the result of the complex interplay and interactions between the four hillslope variables that we tested. The connectivity of large-scale patterns of high relative saturation at the soil–bedrock interface was identified as the unifying emergent feature shaping the generation of fast lateral subsurface stormflow along the soil–bedrock interface.

Fig. 10 summarizes our conceptual model of the interplay between bedrock permeability, slope angle, soil depth and storm size.

Bedrock permeability or the hydraulic conductivity contrast between soil and bedrock are the first discriminating control on hillslope connectivity potential. Slope angle affects the balance between fill and spill processes while soil depth influences the degree and the timing of connectivity. Both factors therefore govern the spatial and temporal distribution of water across the hillslope and resulting flow paths and flow velocities. Storm size has an effect on the occurrence of water ponding as well as on the connectivity.

Our conceptual model visualizes the interplay between fixed slope properties and variable rainfall input characteristics and their control on hydrological connectivity. While we use the DEM and soil properties of a single study hillslope at the Panola Mountain Research Watershed, we argue that this may be a first step in exploring the entire parameter space that comprises hillslope rainfall–runoff response. Overall, our findings suggest that irregular geometries lead to a complex balance of distribution and downslope transport of water. By using a naturally occurring irregular surface and bedrock topography we could show the complexity
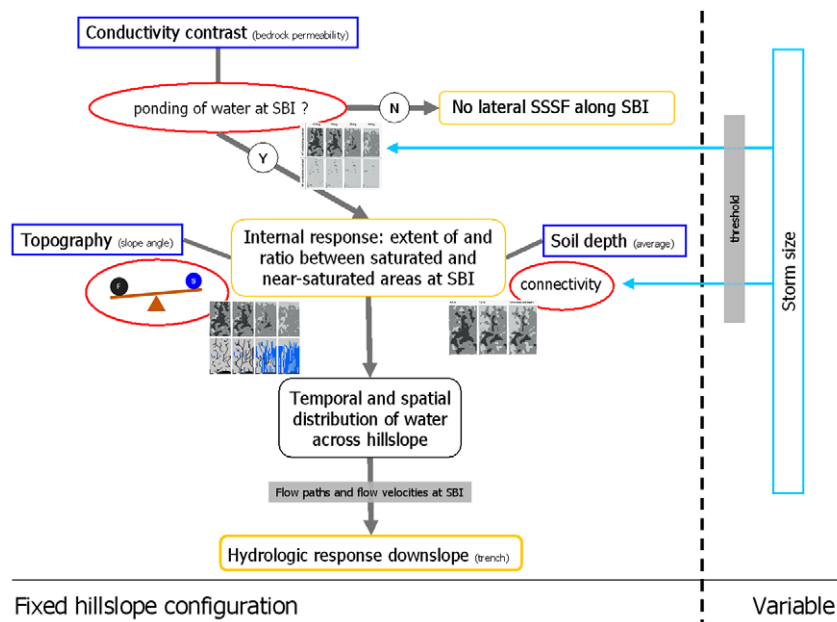

Fig. 10. Conceptual model of interplay between static hillslope attributes and the dynamic variable storm size.

of subsurface flow generation, thereby raising the awareness for the potential occurrence of unexpected non-intuitive behavior in the form of our identified interactions. While physics-based approaches have been applied to experimental slopes in other investigations (e.g. Ebel et al., 2008; Kampf and Burges, 2007) and used in numerical experiments on idealized hillslope geometries (e.g. Fiori and Russo, 2007), they have not yet been used in a virtual experiment mode to explore the interplay of hillslope runoff controls on flow activation. Our work suggests new avenues for use of physics-based simulators to explore new regions of parameter space in helping to ultimately classify slope behavior and begin to build a typology of hillslope response to storm rainfall (as advocated by Wagener et al., 2007).

Conclusions

The limited classification efforts to date in hillslope and watershed hydrology (Wagener et al., 2007) have thus far been based on integrated responses such as discharge (Buttle, 2006). This paper has presented a number of virtual experiments with a 3D physically-based finite element model to systematically investigate the interactions between some of the dominant controls on subsurface stormflow generation. Here we propose the concept of hydrological connectivity – which is a property of the internal spatially distributed state variables – as a possible unifying descriptor and theoretical platform for classification and advancement of understanding of hillslope-scale rainfall–runoff response. Our synthetic work was aimed at understanding the interactions between static hillslope attributes and temporally varying factors and their combined controls on hillslope connectivity. Our findings illustrated the complexity of the interplay between slope angle, soil depth, bedrock permeability and storm size, modulating the balance between fill and spill and the distribution of water across the hillslope. Our conceptual model helps with the generalization of hillslope behavior by showing for the first time, the hierarchy of hillslope variables and their control on hydrological connectivity, driving hillslope rainfall–runoff response. While our hierarchy of controls is likely limited to humid landscapes, it appears that bedrock permeability is a key initial determinant of subsurface threshold response. This implies that characterization of the soil–bedrock permeability contrast may be an important field diagnostic for characterizing hillslope function. Future field and modeling work should be aimed at characterizing other robust measures of hydrological connectivity in diverse hydrological environments.

Acknowledgements

Appendix A. Supplementary material

Supplementary data associated with this article can be found, in the online version, at doi:10.1016/j.jhydrol.2009.07.047.

References

Bracken, L.J., Croke, J., 2007. The concept of hydrological connectivity and its contribution to understanding runoff-dominated geomorphic systems. Hydrological Processes 21, 1749–1763.

Buczko, U., Gerke, H.H., 2006. Modeling two-dimensional water flow and bromide transport in a heterogeneous lignitic mine soil. Vadose Zone Journal 5, 14–26.

Burns, D.A. et al., 2001. Quantifying contributions to storm runoff through end-member mixing analysis and hydrologic measurements at the Panola Mountain Research Watershed (Georgia, USA). Hydrological Processes 15, 1903–1924.

Buttle, J., 2006. Mapping first-order controls on streamflow from drainage basins: the T-3 template. Hydrological Processes 20, 3415–3422.

Buttle, J.M., McDonald, D.J., 2002. Coupled vertical and lateral preferential flow on a forested slope. Water Resources Research 38, 1060. doi:10.1029/2001WR000773.

Buttle, J.M., Dillon, P.J., Eerkes, G.R., 2004. Hydrologic coupling of slopes, riparian zones and streams: an example from the Canadian Shield. Journal of Hydrology 287, 161–177.

Cloke, H.L., Anderson, M.G., McDonnell, J.J., Renaud, J.P., 2006. Using numerical modelling to evaluate the capillary fringe groundwater ridging hypothesis of streamflow generation. Journal of Hydrology 316, 141–162.

Dunne, T., 1978. Field studies of hillslope flow processes. In: Kirkby, M.J. (Ed.), Hillslope Hydrology. John Wiley & Sons, p. 389.

Ebel, B.A., Loague, K., Montgomery, D.R., Dietrich, W.E., 2008. Physics-based continuous simulation of long-term near-surface hydrologic response for the Coos Bay experimental catchment. Water Resources Research 44, W07417. doi:10.1029/2007WR006442.

Fiori, A., Russo, D., 2007. Numerical analyses of subsurface flow in a steep hillslope under rainfall: the role of the spatial heterogeneity of the formation hydraulic properties. Water Resources Research 43, W07445. doi:10.1029/2006WR005365.

Freer, J. et al., 2002. The role of bedrock topography on subsurface storm flow. Water Resources Research 38, 1269. doi:10.1029/2001WR000872.

Gomi, T., Sidle, R.C., Miyata, S., Kosugi, K., Onda, Y., 2008. Dynamic runoff connectivity of overland flow on steep forested hillslopes: scale effects and runoff transfer. Water Resources Research 44, W08411. doi:10.1029/2007WR005894.

Hjerdt, K.N., McDonnell, J.J., Seibert, J., Rodhe, A., 2004. A new topographic index to quantify downslope controls on local drainage. Water Resources Research 40, W05602. doi:10.1029/2004WR003130.

Hutchinson, D.G., Moore, R.D., 2000. Throughflow variability on a forested hillslope underlain by compacted glacial till. Hydrological Processes 14, 1751–1766.

Jenson, S.K., Domingue, J.O., 1988. Extracting topographic structure from digital elevation data for geographic information-system analysis. Photogrammetric Engineering and Remote Sensing 54, 1593–1600.

Kampf, S.K., Burges, S.J., 2007. Parameter estimation for a physics-based distributed hydrologic model using measured outflow fluxes and internal moisture states. Water Resources Research 43, W12414. doi:10.1029/2006WR005605.

Keim, R.F., Meerveld, H., McDonnell, J.J., 2006. A virtual experiment on the effects of evaporation and intensity smoothing by canopy interception on subsurface stormflow generation. Journal of Hydrology 327, 352–364.

Lehmann, P., Hinz, C., McGrath, G., Tromp-van Meerveld, H.J., McDonnell, J.J., 2007. Rainfall threshold for hillslope outflow: an emergent property of flow pathway connectivity. Hydrology and Earth System Sciences 11, 1047–1063.

Lin, H., 2006. Temporal stability of soil moisture spatial pattern and subsurface preferential flow pathways in the shale hills catchment. Vadose Zone Journal 5, 317–340.

McDonnell, J.J. et al., 1996. New method developed for studying flow on hillslopes. EOS, Transactions American Geophysical Union 77, 465.

McDonnell, J.J. et al., 2007. Moving beyond heterogeneity and process complexity: a new vision for watershed hydrology. Water Resources Research 43, W07301. doi:10.1029/2006WR005467.

McIntosh, J., McDonnell, J.J., Peters, N.E., 1999. Tracer and hydrometric study of preferential flow in large undisturbed soil cores from the Georgia Piedmont, USA. Hydrological Processes 13, 139–155.

Mosley, M.P., 1979. Streamflow generation in a forested watershed, New-Zealand. Water Resources Research 15, 795–806.

Onda, Y., Komatsu, Y., Tsujimura, M., Fujihara, J., 2001. The role of subsurface runoff through bedrock on storm flow generation. Hydrological Processes 15, 1693–1706.

Pringle, C.M., 2001. Hydrologic connectivity and the management of biological reserves: a global perspective. Ecological Applications 11, 981–998.

Sansoulet, J., Cabidoche, Y.M., Cattan, P., Ruy, S., Simunek, J., 2008. Spatially distributed water fluxes in an andisol under banana plants: experiments and three-dimensional modeling. Vadose Zone Journal 7, 819–829.

Scherrer, S., Naef, F., 2003. A decision scheme to indicate dominant hydrological flow processes on temperate grassland. Hydrological Processes 17, 391–401.

Simunek, J., van Genuchten, M.T., Sejna, M., 2006. The HYDRUS Software Package for Simulating Two- and Three-dimensional Movement of Water, Heat, and Multiple Solutes in Variably-Saturated Media: Technical Manual. Version 1.0. PC-Progress, Prague, Czech Republic.

Spence, C., 2007. On the relation between dynamic storage and runoff: a discussion on thresholds, efficiency, and function. Water Resources Research 43, W12416. doi:10.1029/2006WR005645.

Spence, C., Woo, M.K., 2006. Hydrology of subarctic Canadian Shield: heterogeneous headwater basins. Journal of Hydrology 317, 138–154.

Tani, M., 1997. Runoff generation processes estimated from hydrological observations on a steep forested hillslope with a thin soil layer. Journal of Hydrology 200, 84–109.

Taylor, P.D., Fahrig, L., Henein, K., Merriam, G., 1993. Connectivity is a vital element of landscape structure. Oikos 68, 571–573.

Tromp-van Meerveld, H.J., McDonnell, J.J., 2006a. Threshold relations in subsurface stormflow: 1. A 147-storm analysis of the Panola hillslope. Water Resources Research 42, W02410. doi:10.1029/2004WR003778.

Tromp-van Meerveld, H.J., McDonnell, J.J., 2006b. Threshold relations in subsurface stormflow: 2. The fill and spill hypothesis. Water Resources Research 42, W02411. doi:10.1029/2004WR003800.

Tromp-van Meerveld, H.J., Peters, N.E., McDonnell, J.J., 2007. Effect of bedrock permeability on subsurface stormflow and the water balance of a trenched hillslope at the Panola Mountain Research Watershed, Georgia, USA. Hydrological Processes 21, 750–769.

Uchida, T., Meerveld, I.T., McDonnell, J.J., 2005. The role of lateral pipe flow in hillslope runoff response: an intercomparison of non-linear hillslope response. Journal of Hydrology 311, 117–133.

van Genuchten, M.T., 1980. A closed-form equation for predicting the hydraulic conductivity of unsaturated soils. Soil Science Society of America Journal 44, 892–898.

van Verseveld, W.J., McDonnell, J.J., Lajtha, K., 2008. A mechanistic assessment of nutrient flushing at the catchment scale. Journal of Hydrology 358, 268–287.

Wagener, T., Sivapalan, M., Troch, P., Woods, R., 2007. Catchment classification and hydrologic similarity. Geography Compass 1, 901–931.

Weiler, M., McDonnell, J., 2004. Virtual experiments: a new approach for improving process conceptualization in hillslope hydrology. Journal of Hydrology 285, 3–18.

Weiler, M., McDonnell, J.J., Tromp van Meerveld, I., Uchida, T., 2005. Subsurface stormflow runoff generation processes. In: Anderson, M.G. (Ed.), Encyclopedia of Hydrological Sciences. John Wiley & Sons, Inc.

Woods, R., Rowe, L., 1996. The changing spatial variability of subsurface flow across a hillside. Journal of Hydrology (New Zealand) 35, 49–84.